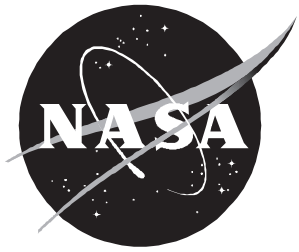

NASA Technical Memorandum 4694

Reflectometer Distance Measurement Between Parallel Conductive Plates

Chase P. Hearn and Robert T. Neece
Langley Research Center • Hampton, Virginia

National Aeronautics and Space Administration
Langley Research Center • Hampton, Virginia 23681-0001

November 1995

Available electronically at the following URL address: http://techreports.larc.nasa.gov/ltrs/ltrs.html

Printed copies available from the following:

NASA Center for AeroSpace Information
800 Elkridge Landing Road
Linthicum Heights, MD 21090-2934
(301) 621-0390

National Technical Information Service (NTIS)
5285 Port Royal Road
Springfield, VA 22161-2171
(703) 487-4650

Abstract

This report presents an analytic and experimental investigation of the measurement problem in which a reflectometer is used to determine the distance to a target that is a highly conductive surface parallel to the reflectometer antenna ground plane. These parallel surfaces constitute a waveguide (WG) which can contribute parasitic perturbations that seriously degrade the accuracy of the measurements. Two distinct parallel-plate-waveguide (PPWG) phenomena are described, and their effects on both frequency and time-domain reflectometers are considered. The time-domain processing approach was found to be superior to a representative frequency-domain phase-measurement approach because of less susceptibility to perturbations produced by edge reflections and immunity to phase capture. Experimental results are presented which show that a simple radiating system modification can suppress parallel-plate (PP) propagation. The addition of a thin layer of lossy mu-metal "magnetic absorber" to the antenna ground plane allowed a measurement accuracy of 0.025 cm (0.01 in.) when a vector network analyzer (VNA) is used as a time-domain reflectometer.

Introduction

Microwave reflectometry can be used to make distance measurements between a directional antenna and a reflecting target. Distance is derived from the complex reflection coefficient, $\Gamma(\omega, d)$, which is measured at the input of the antenna and is a function of both distance d and the radian frequency ω. Such a technique was proposed and developed for measuring the "stand-off" distance between the highly ionized plasma that occurs in front of the heat shield of a reentry vehicle. In this application the plasma may form a highly conductive target parallel to the metallic spacecraft skin. This paper considers the measurement problem in which the reflectometer target is a highly conductive surface parallel to the antenna ground plane, as illustrated in figure 1. These parallel surfaces constitute a parallel-plate waveguide (PPWG) which can contribute parasitic perturbations to $\Gamma(\omega, d)$ that, if ignored, seriously degrade the accuracy of reflectometer measurements (ref. 1). Two distinct PPWG phenomena are described, and their effects on both frequency and time-domain reflectometers are discussed. Techniques for defeating these deleterious mechanisms are presented. Experimental results (of measurements made in a controlled PPWG environment) are presented that yielded distance-measurement accuracies on the order of 0.025 cm (0.01 in.) after the application of these corrective measures.

Symbols

c	velocity of propagation
d	distance
d_u	unambiguous full-scale range
d_0	fixed distance
$F(\omega)$	transfer function
f	frequency
$f(t)$	inverse Fourier transform of $F(\omega)$
$g(t)$	impulse response
k	multiplicative constant
M	magnitude of Γ
m	an integer, 1, 2, 3, ...
n	an integer, 1, 2, 3, ...
Sinc ( )	sin ( )/( )
T_p	propagation time delay, $-\frac{d\Phi}{d\omega}$
V_i	(i = 0, 1, 2, ...)
$W(\omega)$	rectangular frequency domain window $\Delta\omega$ wide centered at ω_0
X,Y,Z	axial coordinates
β	imaginary part of complex propagation constant
$\Gamma(\omega, d)$	complex reflection coefficient dependent on radian frequency and distance
λ	wavelength
λ_0	wavelength of ω_0
ω	radian frequency
ω_m	radian frequency of modulation signal
ω_0	constant radian frequency
$\Phi(\omega, d)$	phase of $\Gamma(\omega, d)$
Φ_D	differential phase between signals at $\omega_0 - \omega_m$ and $\omega_0 + \omega_m$

Abbreviations:

CW	continuous wave
PP	parallel plate
TEM	transverse electromagnetic
TM	transverse magnetic
VES	vector error subtraction
VNA	vector network analyzer
WG	waveguide

Ideal Reflectometer Concept

A reflectometer distance measurement is based on transverse electromagnetic (TEM) wave propagation along the *Z*-axis (fig. 1). With no reflections except the one from the plate and with no parallel-plate (PP) propagation, the phase of $\Gamma(\omega, d)$ at the aperture plane is a linear function of frequency and plate spacing, ω and d, given by

$$\Phi(\omega, d) = -2\beta d = -2\left(\frac{2\pi}{\lambda}\right)d = -\frac{2\omega d}{c} \qquad (1)$$

where β is the imaginary part of the complex propagation constant, λ is the wavelength, and c is the velocity of wave propagation. A fixed-frequency ($\omega = \omega_0$) reflectometer distance measurement based on $\Phi(\omega_0, d)$ becomes ambiguous when $d > \lambda/2$ and Φ exceeds 2π. When $d < \lambda/2$, only the TEM mode can propagate along the *X*- or *Y*-axis and contribute to $\Gamma(\omega_0, d)$. This propagation mode is often ignored in theoretical models because energy loss via radiation is very small if the aperture diameter is at least 1λ (refs. 2 and 3); the measurement of d through $\Phi(\omega, d)$ is nearly ideal.

Multiple *Z*-Axis Reflections

In practice, additional *Z*-axis reflections will occur, as indicated in figure 2. The "local" or first aperture plane reflection V_0 and multiple reflections between the plates (with V_2 the largest) contribute to $\Gamma(\omega_0, d)$. The magnitude and phase functions become nonlinear in d and vary about $-2\omega d/c$ with $\lambda/2$ periodicity (refs. 3 and 4). The local reflection V_0 remains constant as d increases, while V_1 and the multiple reflections decrease. Thus V_0/V_1 increases and V_2/V_1 decreases with d.

Parallel-Plate-Waveguide Effects

When $d > \lambda/2$, a modulated excitation signal can eliminate ambiguity, but PPWG propagation occurs along the *X*- or *Y*-axis. This PPWG propagation affects $\Gamma(\omega)$ and a distance measurement. The effect of PPWG propagation on $\Gamma(\omega, d)$ has been well documented for fixed-frequency ($\omega = \omega_0$) excitation of infinite parallel plates (refs. 1 and 2). It was shown that energy is most efficiently radiated from such systems at plate separations within about $\pm\lambda_0/8$ of

$$d = (2m + 1)\left(\frac{\lambda_0}{4}\right) \qquad (m = 1, 2, 3, \ldots) \qquad (2)$$

and that radiation is ideally zero at the "critical points" that are defined by equation (3).

$$d = n\left(\frac{\lambda_0}{2}\right) \qquad (n = 1, 2, 3, \ldots) \qquad (3)$$

With ω constant, variations in the magnitude and phase of $\Gamma(\omega_0, d)$, which are periodic in $\lambda_0/2$ are observed as d is varied (as sketched in fig. 3). Similar behavior is observed in $\Gamma(\omega, d_0)$, with d fixed and ω varied. The latter case, with ω variable, is of interest here because it is applicable to measuring distances greater than $\lambda/2$.

Each critical point corresponds to the introduction of a new PPWG transverse magnetic (TM) mode (ref. 1). At those points, the new mode in the waveguide (WG) channel presents such a poor match to the aperture plane that the incident wave is largely reflected and radiation is squelched. With d fixed, varying f changes λ. As equations (2) and (3) are alternately satisfied, $\Phi(\omega, d)$ and $M(\omega, d) \equiv |\Gamma(\omega, d)|$ exhibit large periodic variations as the 1-way electrical path length changes by $\lambda/2$. Thus, PPWG propagation imposes a characteristic "signature" (modulation) on $\Gamma(\omega, d)$. This modulation is periodic in $\lambda/2$ and much larger than the modulation that is produced by *Z*-axis multiple reflections. These effects are demonstrated in figure 4. Removal of the ground plane eliminated the PP propagation channel and reduced the $\lambda/2$ variations in $M(\omega_0, d)$ from 17 to 3 dB at $d = 20$ cm. Although PPWG propagation and *Z*-axis multiple reflections disturb $\Gamma(\omega, d)$ with the same periodicity, the wave forms are quite different. Figure 5 compares a typical PPWG response (ref. 2) with the computed vector sum of a primary reflection plus the first multiple reflection (corresponding to V_1 and V_2 in fig. 2).

In theory the PPWG signature intensifies as d and the number of WG modes increase; however, this increase is partially offset in practice by reduced peaks in $M(\omega_0, d)$, as illustrated in figure 4. Reduced deviation of $\Phi(\omega, d)$ from linear was observed to accompany a reduction of PPWG variations in $M(\omega, d)$.

Edge effects in finite PP fixtures produce the rapid fluctuations ("trough ripple") in $\Gamma(\omega_0, d)$ evident in figure 4 and which can affect a distance measurement. Just above its cutoff, the electrical length of a WG for a new mode is very sensitive to d or f. Wave propagation along the *X*- or *Y*-axis in a PPWG is highly mismatched near

WG cutoff (ref. 5). Reflections at the edges of a PP fixture impose a series of "resonant loops" on $\Gamma(\omega, d)$ between critical points. Figures 6 and 7 are from a narrow span which includes only two critical points to illustrate these effects. Dispersion in the interconnecting WG (and horn) and the linear-phase term were empirically removed from $\Phi(\omega, d)$ by using processing features of the Hewlett Packard (HP 8510C) vector network analyzer (VNA). The result shows the remaining deviations of $\Phi(\omega, d_0)$ from linear.

Resonant loops occur when the PPWG presents a high shunt conductance to the aperture plane. This shunt conductance strongly modifies the aperture plane admittance produced by *Z*-axis transverse electromagnetic (TEM) propagation. Complementary (low-conductance) resonances have relatively little shunting effect on the *Z*-axis response. The loops may be over coupled (encircling the origin) or under coupled (nonencircling), as in figure 6 and impose step changes on $\Phi(\omega, d_0)$ and large impulsive "spikes" on the phase delay $-d\Phi/d\omega$, as is evident in figures 7(a) and 7(b). If the trough ripple is ignored, figures 7(a) and 7(b) show the same general behavior that is sketched in figure 5. Therefore, distance measurements where $d > \lambda/2$ based on $\Phi(\omega, d_0)$ or $d\Phi/d\omega$ are affected adversely by PPWG propagation in a way that cannot be completely "averaged out."

In summary, the impediments to making accurate distance measurements beyond $d = \lambda/2$ with a PP reflectometer are (a) local reflections from the aperture plane, (b) multiple reflections between the reflecting plate and the antenna, and (c) two PPWG propagation effects. All impart nonlinearity to $\Phi(\omega, d)$ that is periodic in $\lambda/2$. In addition, dispersion in the interconnecting waveguide adds additional phase nonlinearity.

Local reflections can be negated with a tuner at the input port in a fixed-frequency system (ref. 2). Vector subtraction of the "free-space" response (with no reflecting plate) from a measured response, defined here as vector error subtraction (VES), can negate the contribution of local reflections to $\Gamma(\omega)$ over the operating bandwidth of a modulated system—provided the system is linear in the sense that if input *x* produces output *y*, then input *kx* produces *ky*. More complex error-correcting calibration schemes have been developed that effectively compensate for both *Z*-axis multiple reflections and local reflections (ref. 6).

Numerous systems that have different modulation formats are applicable to making distance measurements when $d > \lambda/2$. Some systems are less susceptible than others to PPWG effects. This difference is shown here by a comparison of two approaches: a frequency-domain phase-measurement approach and the inverse Fourier transform time-domain approach that is used in modern VNA's.

Frequency-Domain Approach

A simple way to extend unambiguous range in the phase-measurement approach is to use double sideband-suppressed carrier modulation (at $\omega = \omega_m$) to generate two continuous wave (CW) signals separated by $2\omega_m$ and measure the differential phase Φ_D that is accumulated by those signals in traversing the path to and from the reflecting plate (ref. 7). In the ideal case of a reflection from one target in a nondispersive media, the phase difference,

$$(\Phi_D)_{\text{IDEAL}} = 2\omega_m\left(\frac{2d}{c}\right) = 2\omega_m T_p \qquad (4)$$

can be determined without ambiguity when $0 < \Phi_D < 2\pi$. It can be seen in equation (4) that $\Phi_D/2\omega_m$ is the two-way time delay T_p.

For an unambiguous full-scale range of d_u, $\Phi_D = 2\pi$ and ω_m is given by

$$(\omega_m)_u = \frac{\pi c}{2d_u} \qquad (5)$$

This approach was found to be highly vulnerable to the effects described previously, and the approach performed poorly in a PP configuration. The phase nonlinearity associated with each sideband caused large variations in $\Phi_D(\omega_0, d)$ around the value given by equation (4). An analysis of two constant-amplitude reflections predicted a phase error given by

$$\left(\Phi_D - 4\omega_m\frac{d}{c}\right) \approx k\ \sin\left(2\omega_m\frac{d}{c}\right)\cos\left(2\omega_0\frac{d}{c}\right) + \ldots \qquad (6)$$

(See ref. 4.) This expression has the same compound periodicity related to ω_0 and ω_m that is observed in laboratory experiments. It was also shown that sweeping the carrier frequency across a bandwidth $\Delta\omega >> \omega_m$ and averaging the resulting phase measurements reduced phase error by the factor $\text{Sinc}(\Delta\omega d/c)$ (ref. 4). This reduction was verified experimentally by stepping the carrier over 51 points within a band $\Delta\omega = 10\omega_m$ (ref. 6).

Examination of phase and phase-delay measurements from several different PP laboratory fixtures revealed that fluctuations in $\Phi(\omega, d)$ and $d\Phi/d\omega$ that were produced by edge reflections were seldom zero mean and hence could not be eliminated completely by averaging. The limited value of averaging is believed to be one weakness of this approach to distance measurement in a PP environment. Another weakness is that amplitude limiting, normally used in a phase-only measurement approach, makes VES inapplicable. This

inapplicability is a severe limitation if the local reflection is sizable compared with the primary reflection, as occurs when the horn aperture is covered with a highly reflective dielectric heat shield (ref. 7). The phase-measurement approach described here is not linear, making VES inapplicable; signal-to-interference ratios of 0 dB result in "phase capture" by the interfering signal, and the average phase delay of the combined signal becomes the one that is associated with the interference instead of with the primary response. It has been shown that a periodicity related to the primary response remains in $\Phi(\omega)$ after phase capture. That periodicity can be exploited to extract target distance in the presence of the larger interfering response (ref. 8).

Time-Domain Approach

Measured frequency response data that are obtained from a real system (either continuous or discrete) over the interval $(\omega_2 - \omega_1) = \Delta\omega$ define a "transfer function" $F(\omega)$, which is assumed to be zero elsewhere. (No physical system can have such a transfer function which produces an output before the input is applied.) The inverse Fourier transform $f(t)$ of the physically unrealizable transfer function $F(\omega)$ is then computed. This "time response" would result if a unit impulse was applied to the input of a system having the frequency response function $F(\omega)$. The time-domain approach differs from the previous approach because it is linear with respect to the amplitude of the reflected signal and uses both the magnitude and phase of $\Gamma(\omega)$. Thus, VES can be used to negate local reflections.

A unit impulse that passes through a purely real, uniform band-pass "window" function $W(\omega)$ having a value of unity within the bands $\pm(\omega_0 \pm\omega/2)$ and zero elsewhere produces the output:

$$g(t) = 2\Delta f \,\mathrm{Sinc}\left(\frac{\Delta\omega t}{2}\right) \cos(\omega_0 t) \qquad (7)$$

Thus, $f(t)$ can be interpreted as the response that Sinc-pulse excitation of the real system would produce. The output response of a system that has a transfer function with constant magnitude M and linear phase across $\Delta\omega$ (simple weighting and delay) to $g(t)$ is $Mg(t - T_p)$, where T_p is the time for a pulse to propagate through the system $-d\Phi/d\omega$. The location of the output-pulse peak $t = T_p$ can be converted to distance if the propagation velocity in the medium is known. In the time-domain distance measurement approach, $\Gamma(\omega, d_0)$ can be thought of as the transfer function between the reflected and forward voltage waves, with T_p the round-trip propagation time $2d/c$. When $\Gamma(\omega, d_0)$ is inverse transformed, reflections V_0 and V_2 (fig. 2) produce interference pulses that are separated from the primary pulse by multiples of T_p. Figure 8 is the corresponding time-response measurement, without linear phase or dispersion extraction, from which figures 6 and 7 were generated. Figure 9 is the same case with linear phase and dispersion extracted. The secondary reflections are easily identified. Increasing $\Delta\omega$ sharpens the time responses and increases time-distance resolution. The time-distance discrimination and linearity characteristics of this approach allow it to operate in the presence of local interference reflections that are larger than the primary response. This discrimination requires that $T_p = 2d/c$ exceed $2/\Delta f$, which is clearly true in figure 8.

The theory of pulse distortion in linear networks can be used to explain how phase and amplitude fluctuations in $\Gamma(\omega, d)$, caused by secondary Z-axis reflections, PP propagation, and dispersion affect the location and amplitude of the time response to a hypothetical Sinc-pulse input. Although the infinite plate PP signature is not a reflection phenomenon, it influences the amplitude and location of the time response much the same as multiple reflections do.

Periodic variations in either $M(\omega)$ or $\Phi(\omega)$ that are caused by multiple reflections, PPWG propagation, and dispersion give rise in the inverse transform to "echo-pulse" pairs which have the same envelope function as the undistorted output pulse $Mg(t - T_p)$, but which are displaced symmetrically around $Mg(t - T_p)$ by integral multiples of a factor k which defines the "periodicity" of the frequency-domain variations (ref. 9); that factor is T_p for the variations caused by multiple reflections and PPWG propagation and is therefore d dependent.

Uncorrected phase dispersion in the interconnecting waveguide, transition, and horn also introduces nonlinearity to $\Phi(\omega)$—unrelated to T_p—which must be largely eliminated either in hardware or software. When the phase curvature that results from uncorrected dispersion exceeds approximately a radian at the band edges of $\Phi(\omega)$, relative to midband, the time response becomes noticeably smeared, the side-lobe levels increase, and side-lobe symmetry and null depth are reduced, as illustrated in figures 8 and 9. It will be shown that odd-order dispersion produces a fixed-time shift of the envelope peak. These effects did not discernibly degrade the accuracy of time-domain measurements when the total residual dispersion did not exceed a radian; however, dispersion on the order of 4 to 5 rad significantly degraded measurement accuracy.

In a physically realizable, time-invariant linear system, variations in $M(\omega)$ are accompanied by variations in $\Phi(\omega)$. Both variations contribute to time response; their combined effect is to reduce one echo pulse and increase the other. The side lobes of the echo-pulse envelopes interact with the main lobe of the primary pulse to

produce a sum response in which both the amplitude and position of the envelope peak can vary, relative to the primary pulse alone (ref. 9). The PPWG propagation was consistently observed to affect $\Gamma(\omega, d)$ much more strongly than could be attributed solely to *Z*-axis multiple reflections and is therefore the largest contributor to sidelobe interference and measurement error.

A previous study (ref. 9) of the effects of small variations in $M(\omega)$ and $\Phi(\omega)$ on the time response revealed that variations in $M(\omega)$ do not produce time shift, but variations in $\Phi(\omega)$ can. An approximate time response for a frequency-response function having $M(\omega) = 1$ and

$$\Phi(\omega, T_p) = -\omega T_p + \Delta\Phi \sin(\omega T_p) \tag{8}$$

can be derived symbolically when $\Delta\Phi < 1$. The basic form of the result depends on whether the variation term in equation (8) has even or odd symmetry over $\Delta\omega$ with respect to midband $(\omega_1 + \omega_2)/2$ and that symmetry changes when $\omega_0 T_p$ changes by $\pi/2$, as illustrated in figure 10. With even symmetry $\omega_0 T_p = (2n + 1)(\pi/2)$, and

$$f(t) = 2\Delta f \left| \mathrm{Sinc}\left[\frac{\Delta\omega(t - T_p)}{2}\right] \cos[\omega_0 (t - T_p)] + (-1)^m \left(\frac{\Delta\Phi}{2}\right) \left\{ \mathrm{Sinc}\left(\frac{\Delta\omega t}{2}\right) + \mathrm{Sinc}\left[\frac{\Delta\omega(t - 2T_p)}{2}\right] \right\} \sin[\omega_0 (t - T_p)] \right| \tag{9}$$

The echo-pulse and primary-pulse carriers are orthogonal, and the two echo pulses have a combined envelope function that has even symmetry about $t = T_p$. Therefore, the root-squared sum envelope function of $f(t)$ has even symmetry about $t = T_p$, and there is no time shift.

With odd symmetry $\omega_0 T_P = m\pi$ and

$$f(t) = 2\Delta f \left| \mathrm{Sinc}\left[\frac{\Delta\omega(t - T_p)}{2}\right] + (-1)^{m+1} \left(\frac{\Delta\Phi}{2}\right) \left\{ \mathrm{Sinc}\left(\frac{\Delta\omega t}{2}\right) - \mathrm{Sinc}\left[\frac{\Delta\omega(t - 2T_p)}{2}\right] \right\} \right| \cos[\omega_0 (t - T_p)] \tag{10}$$

The envelope functions of the echo and primary pulses add directly because they have inphase carriers. Figure 11 shows the pulse orientations with *m* even and $\Delta\omega T_p/2 = 3\pi$. At $t = T_p$ the combined echo-pulse envelope function changes sign and adds to the primary-pulse envelope on the high side of T_p and subtracts on the low side, producing a positive time shift of the sum-process envelope. When T_p is increased so that $\Delta\omega T_p/2 = 4\pi$, the time shift is negative. Time shift can be quantified by representing the three components of the envelope function in equation (10) as Taylor series approximations about $t = T_p$, carrying terms only through the second order. The resulting quadratic approximation for $f(t)$ has a maximum at

$$t_M \approx T_p + (-1)^n \frac{12\Delta\Phi}{n\pi\Delta\omega} \tag{11}$$

where *n* is the order of the echo-pulse zero crossing at $t = T_p$.

When $\Delta\omega T_p/2 = (2n + 1)\pi/2$, the echo pulses have local extremes at $t = T_p$; time shift is zero but the sum-pulse amplitude has a local extreme value. The extremes of the amplitude and position errors alternate and follow a downward trend as T_p increases.

In summary, as $T_p = 2d/c$ changes, the measurement error exhibits compound periodicity as the parameters that control the relative orientation of the primary and echo-pulse lobes $\Delta\omega T_p/2$, and the phase difference between the primary and echo-pulse carriers $\omega_0 T_p$ change by 2π. Increasing $\Delta\omega$ causes the measurement error to follow a downward trend. These are the same general conclusions that were drawn earlier for the frequency-domain approach.

Time-domain measurements were affected less by trough ripple than frequency-domain measurements were. This difference probably occurs because the variations in $\Gamma(\omega)$ that are produced by trough ripple change rapidly with ω and are widely dispersed in the time-domain transformation; relatively little interference is contributed to the critical region that contains the main lobe of the primary pulse.

Reduction of PPWG Effects

Any measure that can reduce PPWG disturbances without significantly affecting the primary *Z*-axis reflection reduces the periodic variations of $\Phi(\omega)$ from linear, the resulting time-shift of the time-domain sum pulse, and therefore the measurement error. Two effective methods for reducing PP effects were found. First, adding a slight curvature to one of the surfaces can corrupt the PP geometry sufficiently to completely squelch PPWG propagation—with negligible reduction of the primary response. This suppression was demonstrated with a 25.4-cm (10-in.) square PP fixture operating at 16 ± 2 GHz that was modified to have a curvature radius of 58.4 cm (23 in.) on the reflecting plate. For any value of *d*, there was a circular locus in the *X*-*Y* plane along which the plate spacing *d* would satisfy equation (3) and squelch propagation.

Secondly, a 10-mm (0.04-in.) layer of commercially available magnetic absorber on the ground plane was used to negate substantially the electrical effect of the ground plane. This absorber consists of lossy mu-metal particles suspended in Rutile and also is available in a paint-on medium (ref. 10). Measurements with several different test fixtures operating in the 14- to 26-GHz region showed that applying this material around the horn aperture reduced the secondary pulse by 6 to 14 dB while reducing the primary pulse amplitude only 0.2 dB. When the aperture plane reflection, in V_0 figure 2, is negligibly small or when VES is used, distance-measurement error was observed to be closely proportional to V_2/V_1. A ring of magnetic absorber that covered the ground plane to about 6λ beyond the perimeter of a 5λ horn effectively suppressed PPWG contributions to $\Gamma(\omega, d)$, leaving only Z-axis local and multiple reflections to corrupt the measurement. These tests were not extensive; even less absorber coverage might adequately suppress PPWG propagation.

Test Results

The results of time-domain delay measurements using an HP 8510C as a reflectometer and a precision PP fixture having 36λ square plates fed by a 5λ circular horn are shown in figure 12. The local reflection was about 35 dB below the incident wave and 20 dB below the primary reflection; VES was therefore of little benefit. With 10-mm (0.04-in.) magnetic absorber over the ground plane (using 801 points across a 4-GHz span), deviations of the measured "round-trip" time delay from a straight line of slope 0.067 ns/cm (0.1693 ns/in.) were no more than ±3 ps for plate spacings between 0 and 38 cm (15 in.)—a 1-way distance-measurement error of less than 0.051 cm (0.02 in.). Removal of the absorber increased that error fivefold.

These results were obtained without using nonuniform windowing for side-lobe suppression. Windowing drastically increased measurement error below some minimum value of pulse separation and plate spacing (ref. 11). With a 4-GHz span, the HP 8510C "normal" window increased measurement error for plate separations less than 8.26 cm (3.25 in.) but reduced error appreciably for larger separations. This effect was interpreted to be a consequence of the pulse broadening which accompanies windowing. Windowing becomes detrimental when the "broadened" main lobes of the signal and interference pulses interact with each other.

Conclusions

The accuracy of microwave reflectometer measurements of the distance between conductive parallel plates is reduced by parallel-plate-waveguide (PPWG) propagation in the parallel-plate (PP) channels perpendicular to the measurement axis. These additional propagation channels influence $\Gamma(\omega, d)$ and distance measurements derived from it. A simple radiating system modification which can suppress parallel-plate propagation is the addition of a thin layer of lossy mu-metal "magnetic absorber" to the antenna ground plane. With this modification, a measurement accuracy of 0.025 cm (0.01 in.) was obtained using an HP 8510C as a time-domain reflectometer.

The time-domain processing approach was superior to a representative frequency-domain phase-measurement approach because of (a) less susceptibility to the trough ripple that is produced by edge reflections in a PP environment, (b) immunity to phase capture, and (c) the applicability of vector error subtraction. Time did not permit a thorough evaluation of the comparative performance of the two approaches in the absence of PPWG propagation; however, both approaches benefited directly from increasing the operating bandwidth $\Delta\omega$.

NASA Langley Research Center
Hampton, VA 23681-0001
August 11, 1995

References

1. Jones, J. Earl; and Swift, C. T.: *The Aperture Admittance of a Ground-Plane-Mounted Waveguide Illuminating a Perfectly Conducting Sheet*. NASA TN D-4366, 1968.

2. Bailey, M. C.: *CWG: A FORTRAN Program for Mutual Coupling in a Planar Array of Circular Waveguide-Fed Apertures*. NASA TM-101614, 1989.

3. Hearn, C. P.; Bailey, M. C.; Czerner, M. J.; Dudley, K. L.; and Vedeler, E.: *An Assessment of the Potential of Continuous-Wave Ranging for Measuring the Distance to a Highly Reflective, Infinite Sheet*. NASA TM-101680, 1990.

4. Hearn, C. P.; Cockrell, C. R.; and Harrah, S. D.: *An Analysis of the Effects of Secondary Reflections on Dual-Frequency Reflectometers*. NASA TM-102709, 1990.

5. Ryder, John Douglas: *Networks, Lines, and Fields*. Prentice-Hall Publ., 1949.

6. Seals, Joseph; Fordham, Jeffrey A.; Pauley, Robert G.; and Simonutti, Mario D.: *Microwave Reflectometer Ionization Sensor*. NASA CR-191464, 1993.

7. Neece, Robert T.; Cross, Aubrey E.; and Schrader, James H.: *The MRIS Feasibility Study*. NASA TM-107763, 1993.

8. Ybarra, Gary A.; Ardalan, Sasan H.; Hearn, Chase P.; Neece, Robert T.; and Marshall, Robert E.: Detection of Target Distance in the Presence of an Interfering Reflection Using a Frequency-Stepped Double Side-Band Suppressed Carrier Microwave Radar System. *IEEE Trans. Microw. Theory & Tech.*, vol. 39, May 1991, pp. 809–818.

9. Sunde, Erling Ditlef: *Communication Systems Engineering Theory*. John Wiley & Sons, Inc., 1969.

10. *Microwave Absorbers*. GEC-Marconi Materials, San Diego, CA, Sept. 1991.

11. Hearn, Chase P.: Study Examines Windowing Effects on VNA Measurements. *Microw. & RF*, vol. 33, no. 9, Sept. 1994, pp. 108–110.

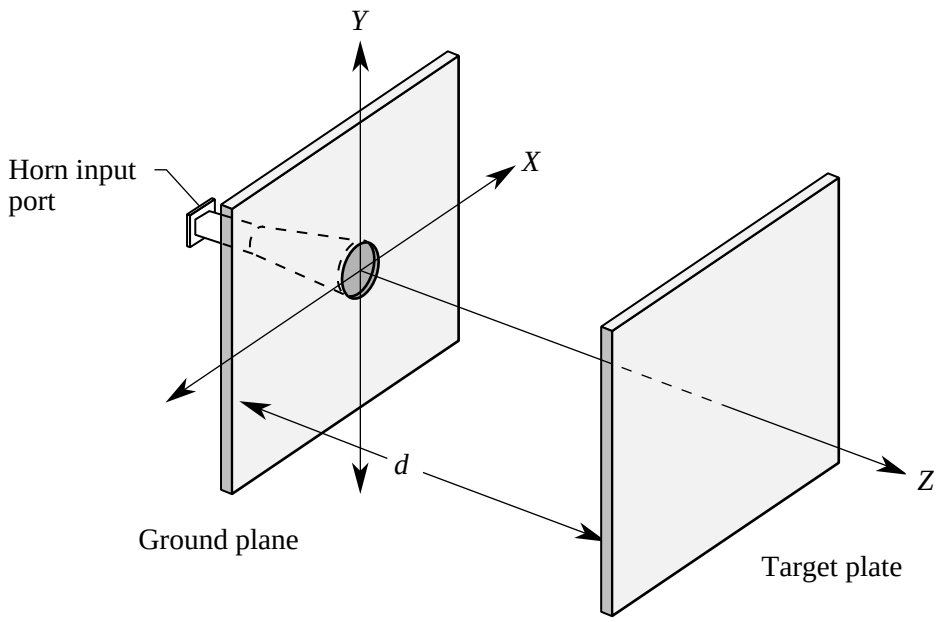

Figure 1. Waveguide-fed, parallel-plate system.

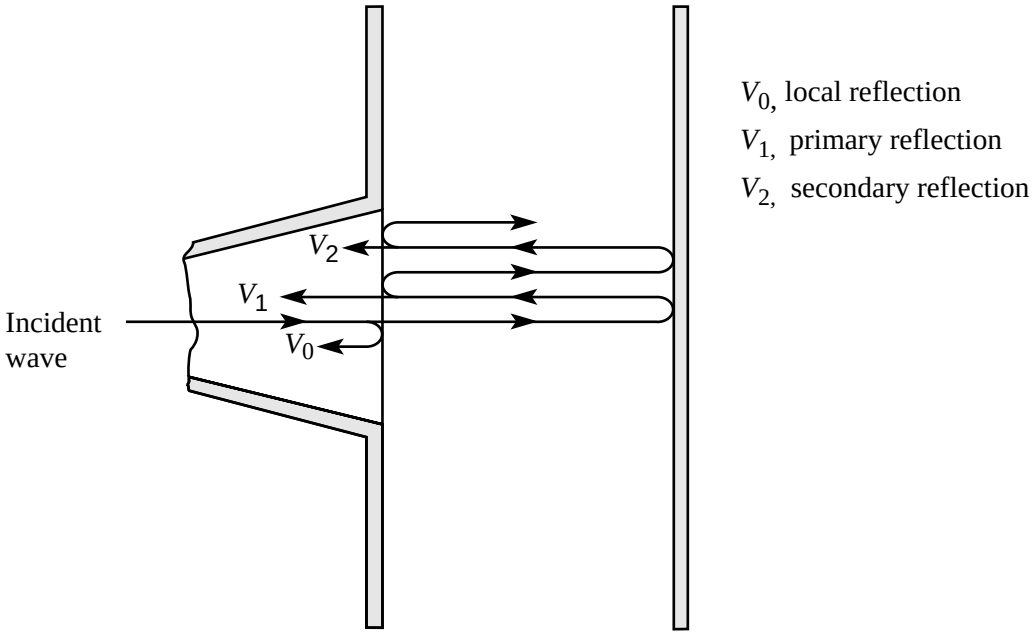

Figure 2. Local, primary, and secondary reflections in a PP reflectometer.

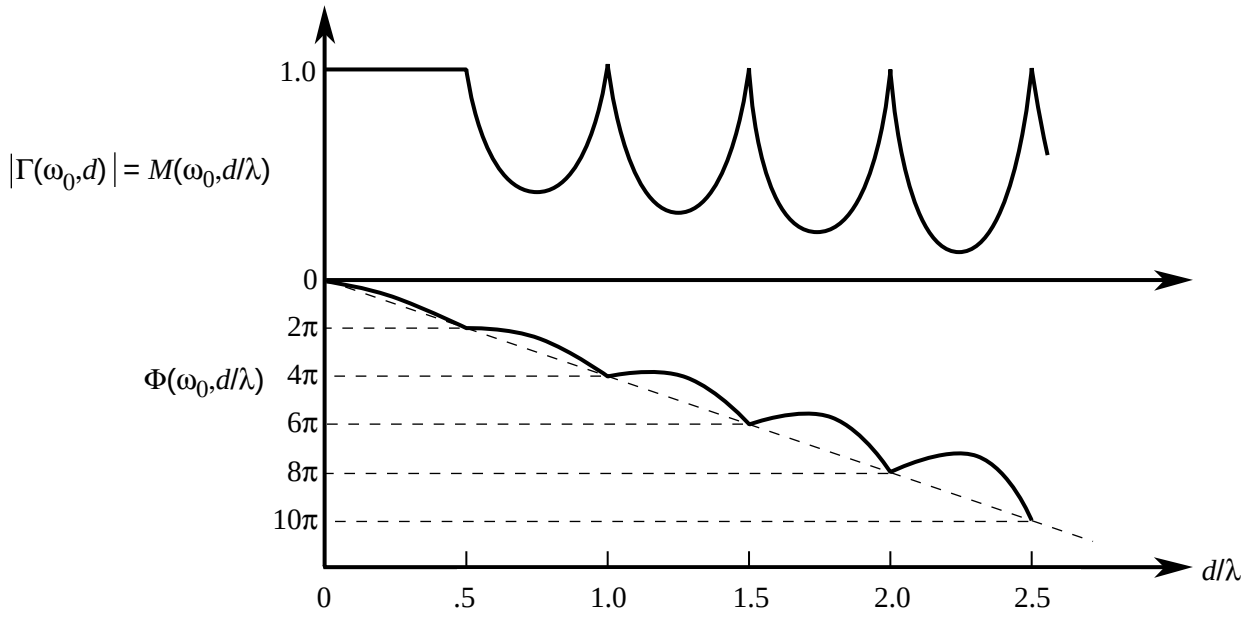

Figure 3. Characteristic behavior of $\Gamma(\omega_0, d)$ in an ideal parallel-plate system.

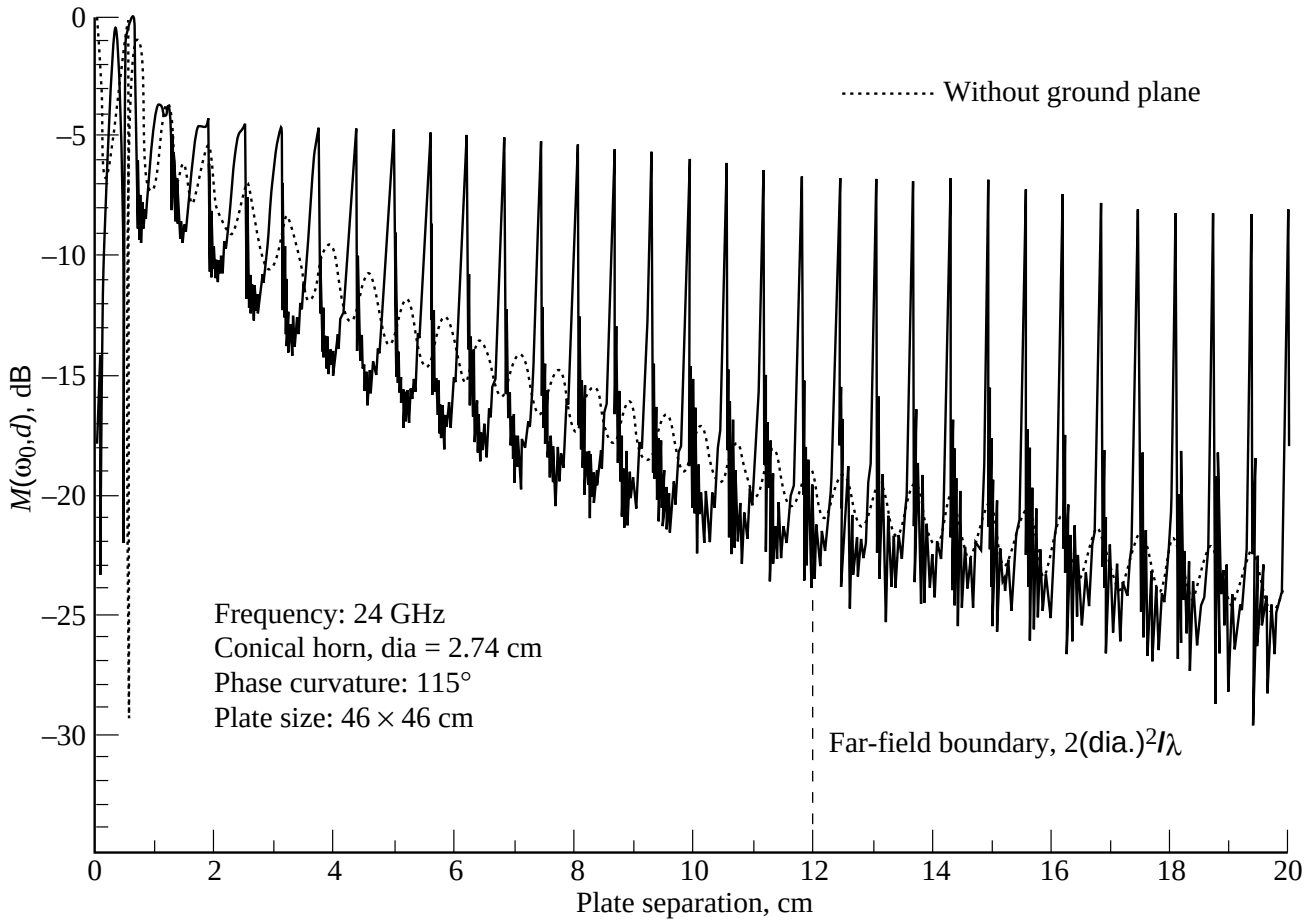

Figure 4. Effect of antenna ground-plane removal on the reflection coefficient magnitude.

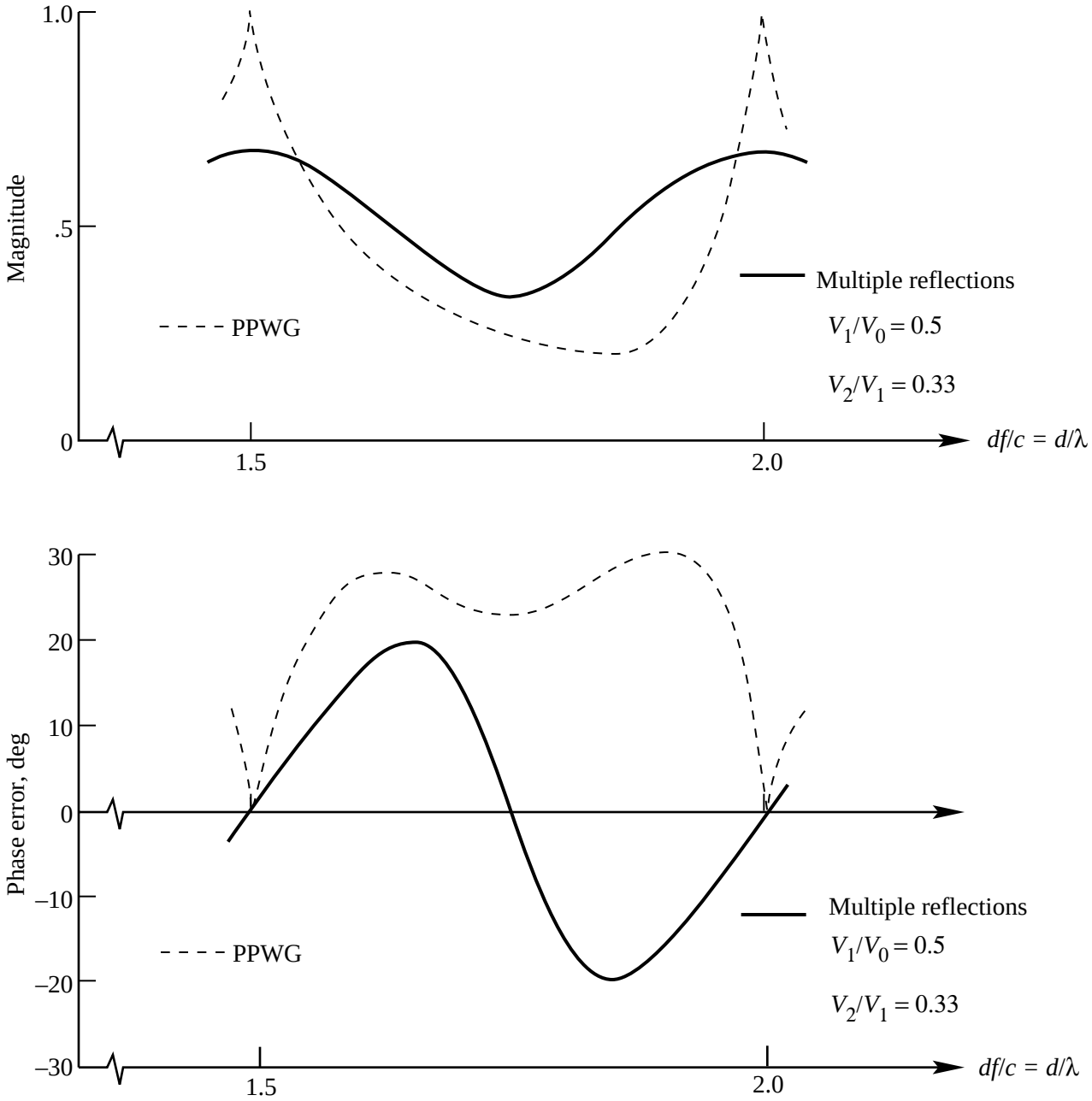

Figure 5. Comparison of PPWG and multiple-reflection signatures.

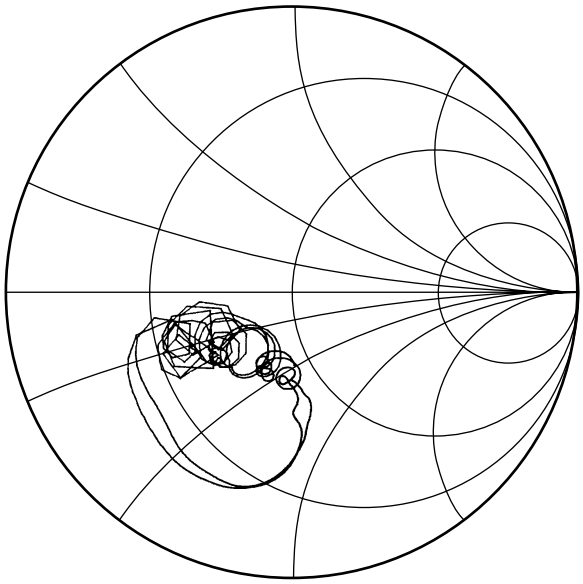

Start frequency 14.800 GHz
Stop frequency 15.800 GHz

Figure 6. Smith-chart plot of $\Gamma(\omega, d_0)$ between critical points, with linear phase term extracted.

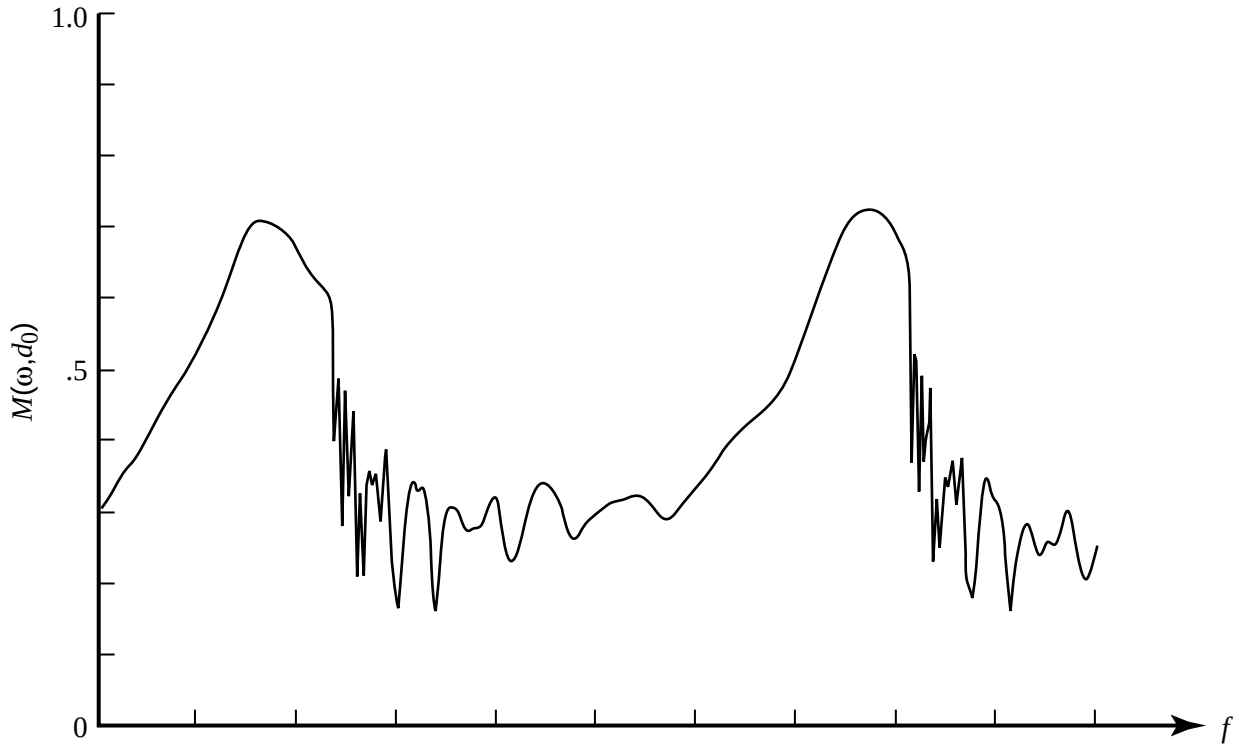

Start frequency 14.965 GHz
Stop frequency 15.570 GHz

(a) Magnitude response.

Figure 7. “Trough ripple” effects.

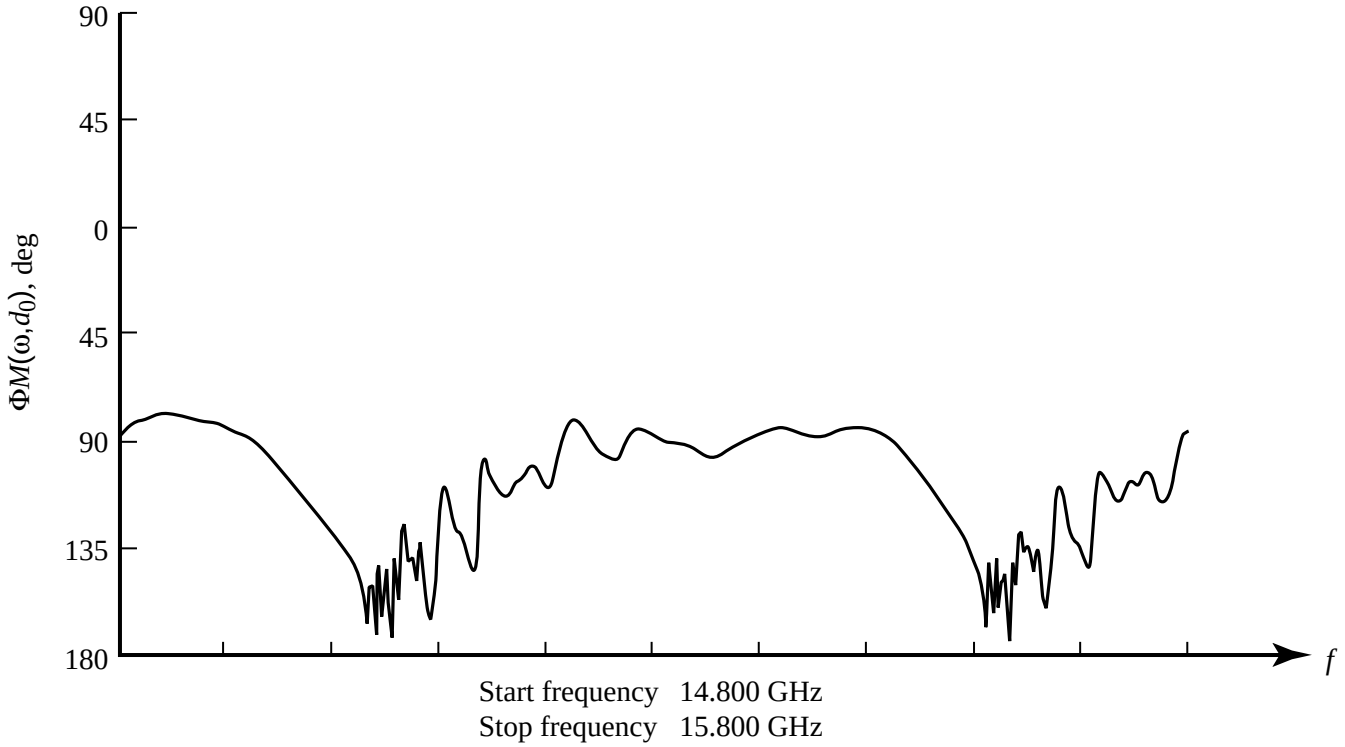

(b) Phase response with linear phase term extracted.

Figure 7. Continued.

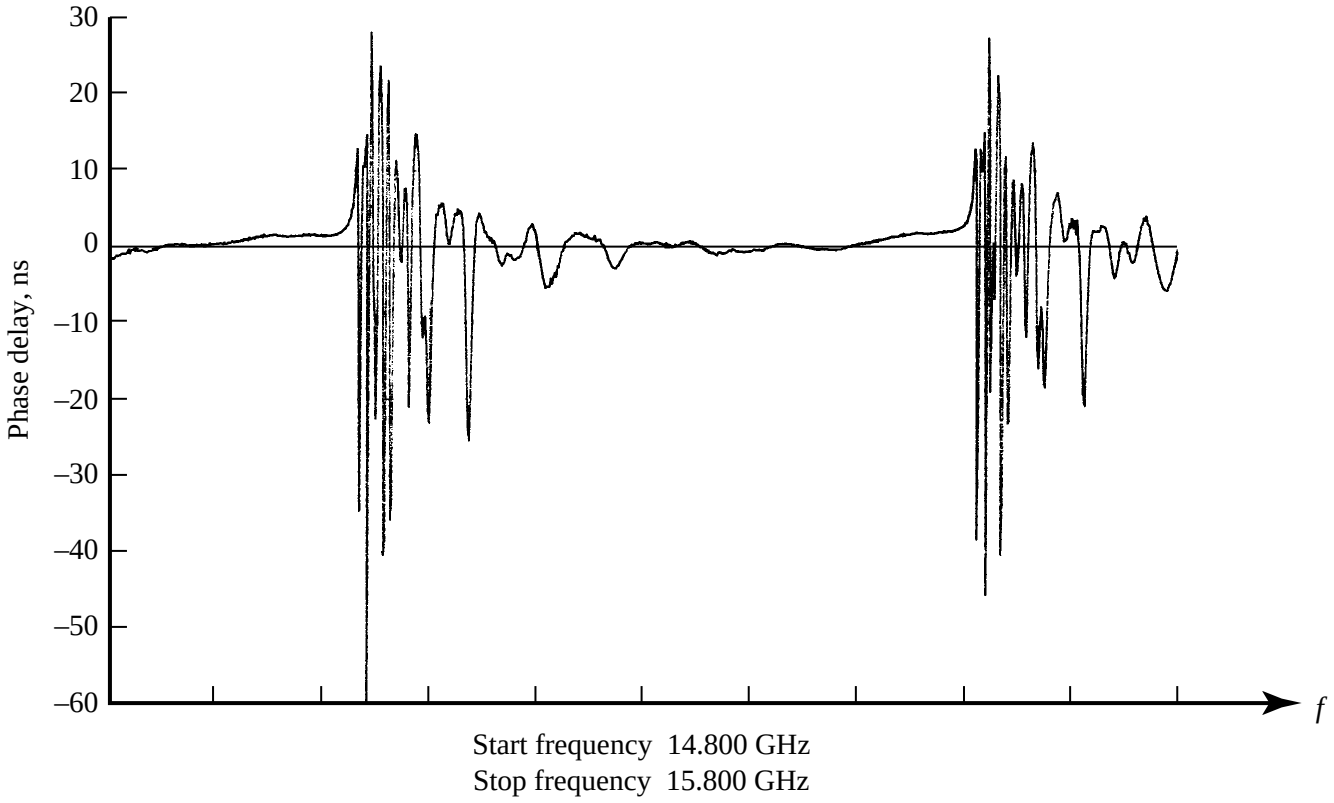

(c) Phase delay response with linear phase term extracted.

Figure 7. Concluded.

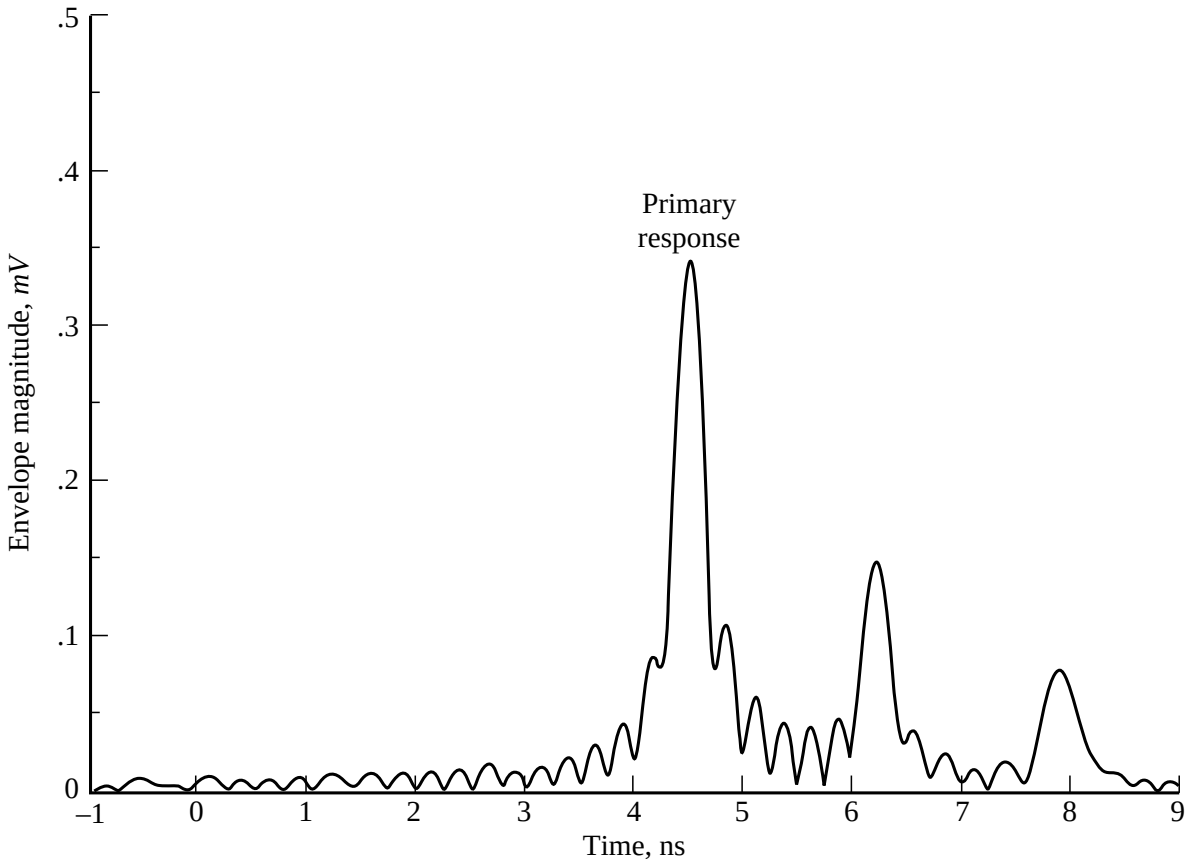

Figure 8. Measured time response (without linear phase or dispersion removal); d = 25.9 cm (10.2 in.).

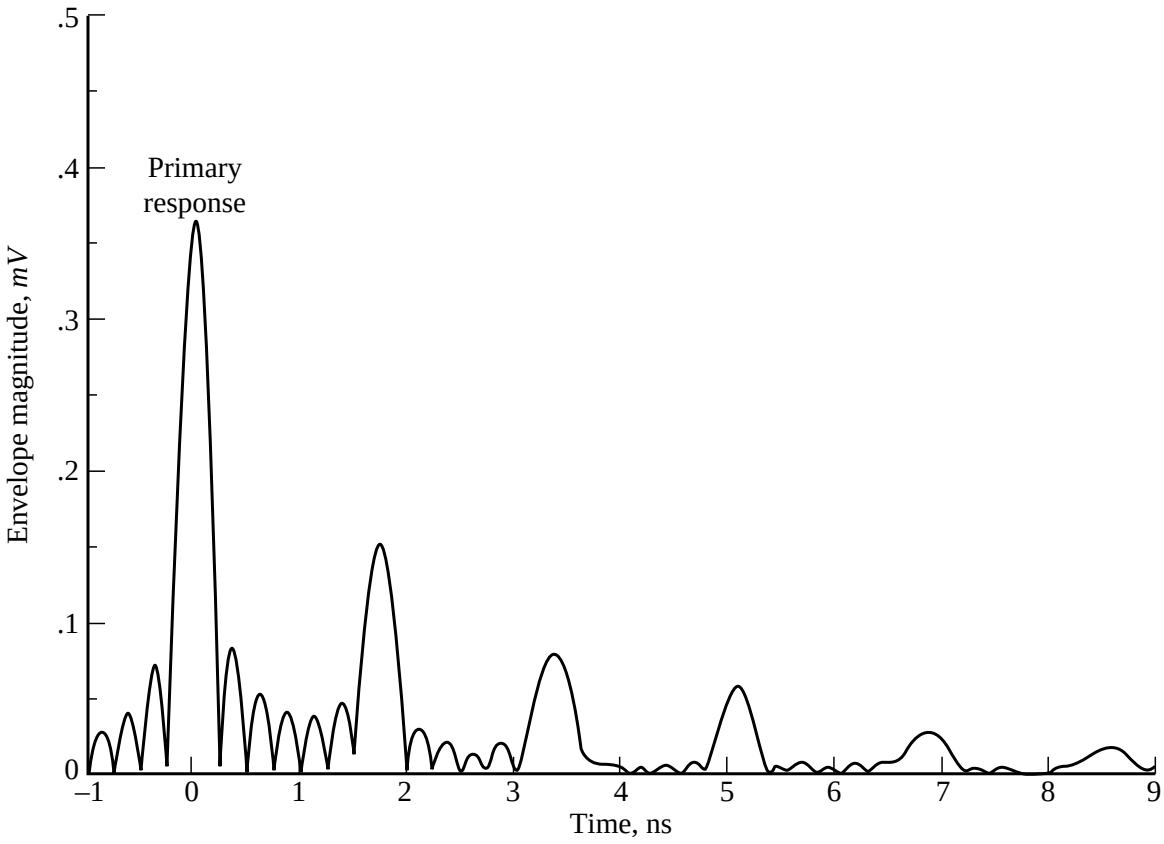

Figure 9. Measured time response with linear phase and dispersion extracted; d = 25.9 cm (10.2 in.).

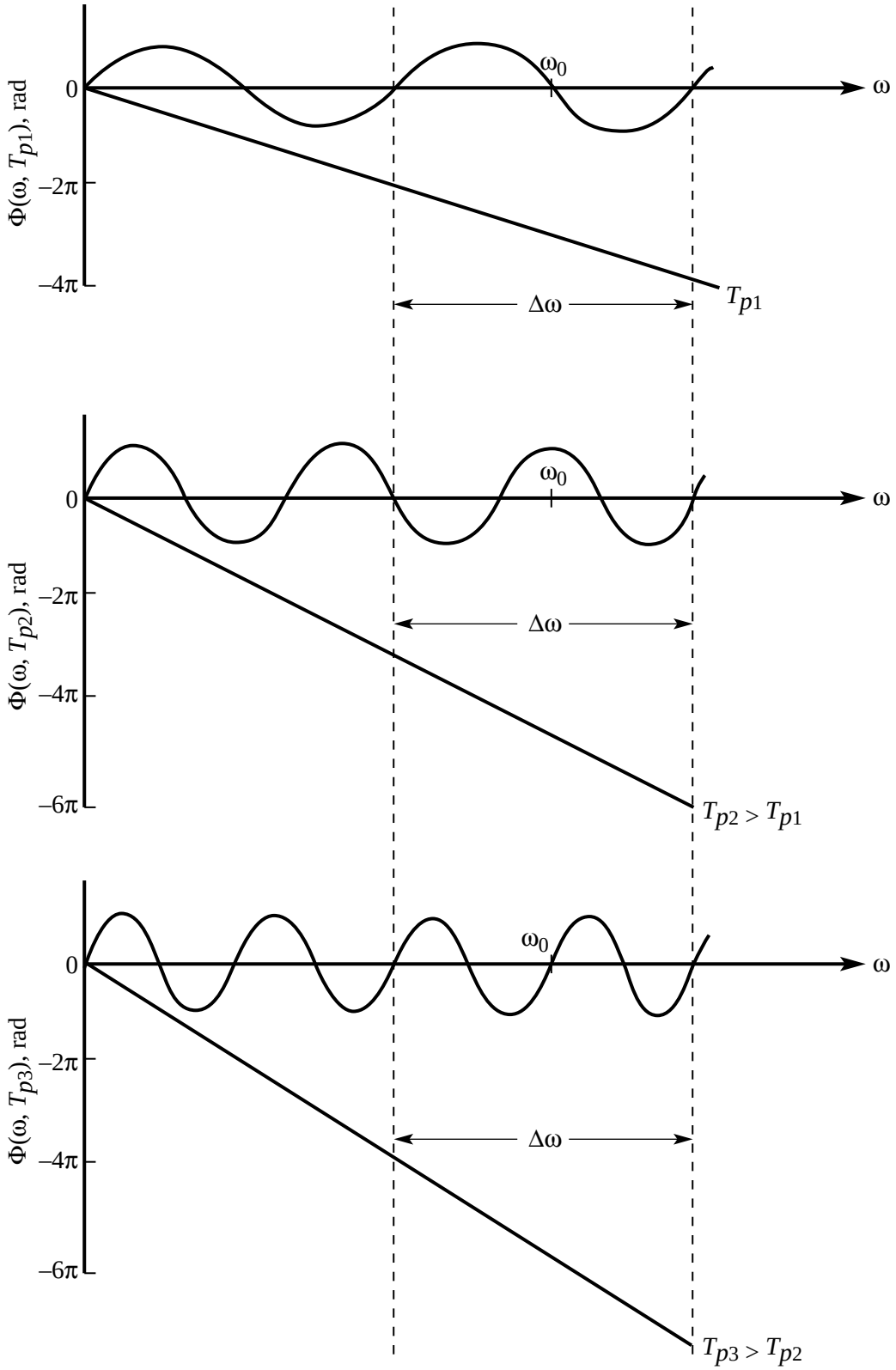

Figure 10. Illustrations of the components of the phase function $\Phi(\omega,T_p) = -\omega T_p + \Delta\Phi \sin\omega T_p$ as T_p is varied.

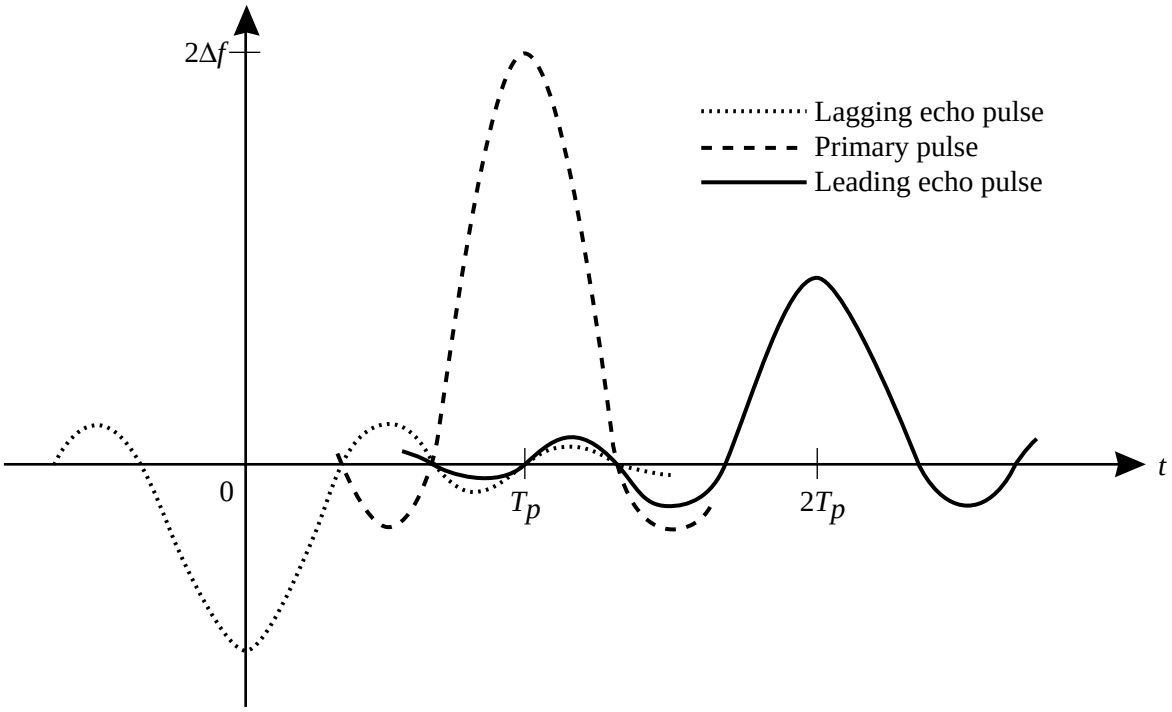

Figure 11. Echo-pulse side-lobe interference producing a positive time shift.

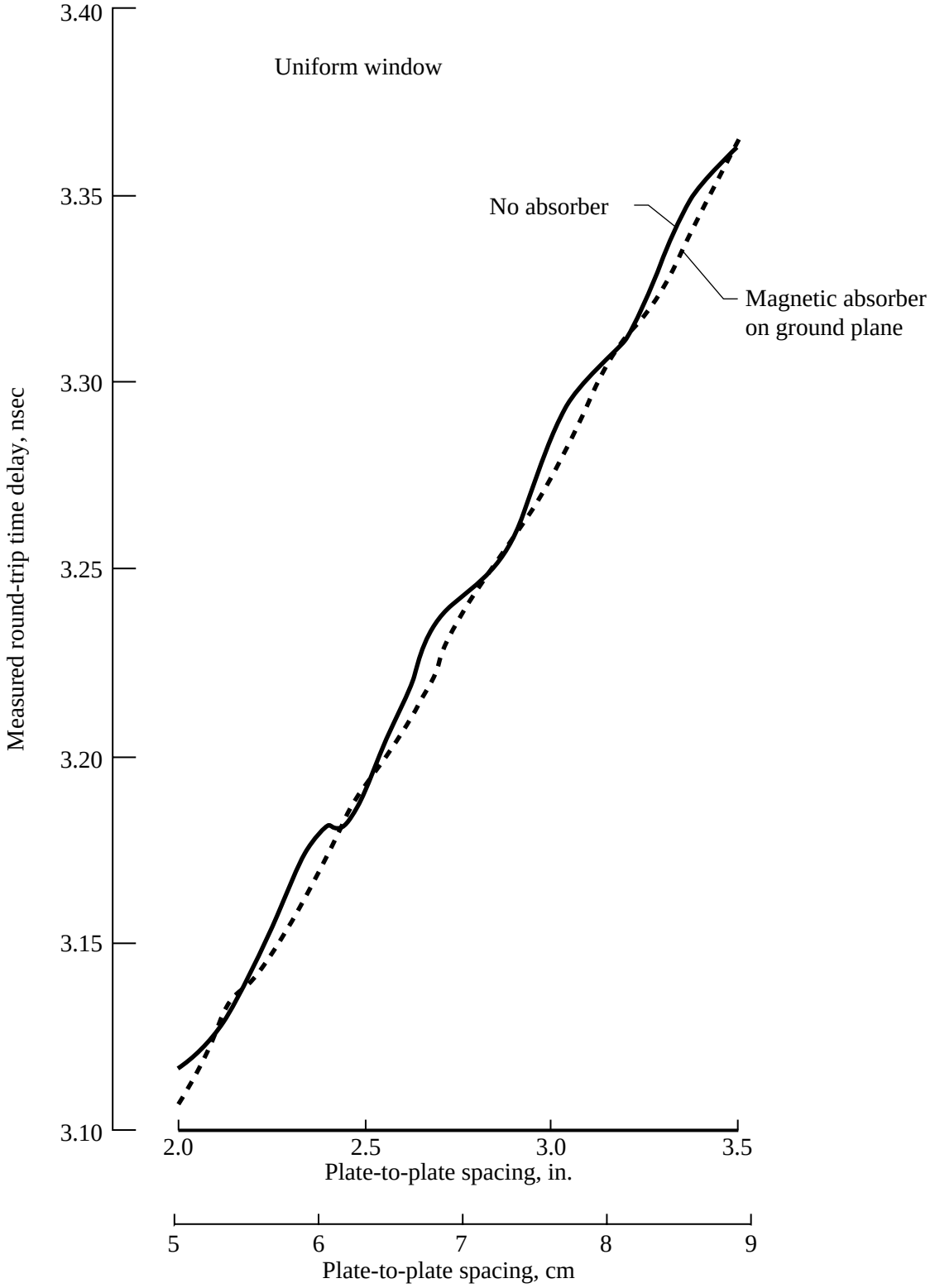

Figure 12. Delay measurements on a parallel-plate test fixture using an HP 8510C as a reflectometer.

REPORT DOCUMENTATION PAGE

Form Approved
OMB No. 0704-0188

1. AGENCY USE ONLY *(Leave blank)*	2. REPORT DATE	3. REPORT TYPE AND DATES COVERED
	November 1995	Technical Memorandum

4. TITLE AND SUBTITLE
Reflectometer Distance Measurement Between Parallel Conductive Plates

5. FUNDING NUMBERS
WU 538-04-11

6. AUTHOR(S)
Chase P. Hearn and Robert T. Neece

7. PERFORMING ORGANIZATION NAME(S) AND ADDRESS(ES)
NASA Langley Research Center
Hampton, VA 23681-0001

8. PERFORMING ORGANIZATION REPORT NUMBER
L-17466

9. SPONSORING/MONITORING AGENCY NAME(S) AND ADDRESS(ES)
National Aeronautics and Space Administration
Washington, DC 20546-0001

10. SPONSORING/MONITORING AGENCY REPORT NUMBER
NASA TM-4694

11. SUPPLEMENTARY NOTES

12a. DISTRIBUTION/AVAILABILITY STATEMENT
Unclassified–Unlimited
Subject Category 32
Availability: NASA CASI (301) 621-0390

12b. DISTRIBUTION CODE

13. ABSTRACT *(Maximum 200 words)*

This report presents an analytic and experimental investigation of the measurement problem in which a reflectometer is used to determine the distance to a target that is a highly conductive surface parallel to the reflectometer antenna ground plane. These parallel surfaces constitute a waveguide (WG) which can contribute parasitic perturbations that seriously degrade the accuracy of the measurements. Two distinct parallel-plate-waveguide (PPWG) phenomena are described, and their effects on both frequency and time-domain reflectometers are considered. The time-domain processing approach was found to be superior to a representative frequency-domain phase-measurement approach because of less susceptibility to perturbations produced by edge reflections and immunity to phase capture. Experimental results are presented which show that a simple radiating system modification can suppress parallel-plate (PP) propagation. The addition of a thin layer of lossy mu-metal “magnetic absorber” to the antenna ground plane allowed a measurement accuracy of 0.025 cm (0.01 in.) when a vector network analyzer (VNA) is used as a time-domain reflectometer.

14. SUBJECT TERMS	15. NUMBER OF PAGES
Microwave reflectometer distance measurement	20
	16. PRICE CODE: A03

17. SECURITY CLASSIFICATION OF REPORT	18. SECURITY CLASSIFICATION OF THIS PAGE	19. SECURITY CLASSIFICATION OF ABSTRACT	20. LIMITATION OF ABSTRACT
Unclassified	Unclassified	Unclassified	